Cross-field electron transport induced by a rotating spoke in a cylindrical Hall thruster

C. L. Ellison, Y. Raitses, and N. J. Fisch
Princeton Plasma Physics Laboratory, Princeton, New Jersey 08543, USA

(Received 17 August 2011; accepted 2 November 2011; published online 12 January 2012)

Rotating spoke phenomena have been observed in a variety of Hall thruster and other $\mathbf{E} \times \mathbf{B}$ devices. It has been suggested that the spoke may be associated with the enhancement of the electron cross-field transport. In this paper, the current conducted across the magnetic field via a rotating spoke has been directly measured for the first time in the $\mathbf{E} \times \mathbf{B}$ discharge of a cylindrical Hall thruster. The spoke current was measured using a segmented anode. Synchronized measurements with a high speed camera and a four-segment anode allow observation of the current as a function of time and azimuthal position. Upwards of 50% of the total current is conducted through the spoke, which occupies a quarter of the Hall thruster channel area. To determine the transport mechanism, emissive and Langmuir probes were installed to measure fluctuating plasma potential, electron density, and temperature. A perturbed, azimuthal electric field and density are observed to oscillate in-phase with the rotating spoke. The resulting drift current is found to enhance electron transport with a magnitude equal to the spoke current to within margins of error. © *2012 American Institute of Physics*. [doi:10.1063/1.3671920]

I. INTRODUCTION

Cross-field transport is of fundamental interest in a variety of devices, including magnetically confined fusion plasmas, Penning traps, magnetrons, and Hall thrusters.[1–4] In addition to classical collisional transport, electron mobility may be enhanced by electron-wall interactions,[5] fluctuations,[6–9] and turbulence.[10]

In the Hall thruster, cross-field transport is of practical importance because it diminishes thruster efficiency. Hall thrusters typically consist of an annular channel in which a radial magnetic field confines electrons, while an axial electric field accelerates ions. A cathode neutralizer maintains neutrality throughout the plasma, mitigating space charge limitations present in other plasma thrusters. A higher specific impulse compared to electrothermal thrusters and larger thrust-per-mass ratio compared to electrostatic ion thrusters makes Hall thrusters preferable candidates for orbital correction and light-weight space missions, such as the SMART-1 European Space Agency mission.[11]

While annular Hall thrusters have successfully operated in the kW power range, the cylindrical Hall thruster (CHT) has been proposed for efficient scaling to low (100–200 W) power levels.[12] In this configuration, the central portion of the annular channel is eliminated, forming a mirror field within a cylindrical channel. The electrons are confined on the near-anode side by the mirror force and on the cathode side by the axial electric field. The decreased surface area of the cylindrical shape is intended to enhance performance by minimizing electron-wall interactions. Like the annular Hall thruster, the CHT exhibits anomalous levels of cross-field transport.[13] The CHT exhibits surprisingly narrow plume divergence, in part due to the rapidly $\mathbf{E} \times \mathbf{B}$ rotating electrons.[14]

A rotating spoke of light has been observed in annular[15–18] and cylindrical[19] Hall thruster geometries, as well as in more general $\mathbf{E} \times \mathbf{B}$ devices.[20] Early studies used electrostatic probes to measure fluctuating density and potential, and inferred the spoke to be contributing to the anomalous transport.[15] The magnitude of the fluctuations appeared to be on the correct order to explain the anomalously high levels. A similar use of emissive probes have observed rotation in a more recent study,[21] though the measurements were performed at low discharge voltage (200 V) and the unclear azimuthal behavior combined with a counter-$\mathbf{E} \times \mathbf{B}$ rotation direction make comparisons with past results difficult. Imaging of annular thruster ignition has revealed azimuthal behavior, which may also be related to the rotating spoke.[22]

Recently, Parker *et al*. observed a 15–35 kHz rotating spoke on the cylindrical Hall thruster using a fast camera and electrostatic probe diagnostics.[19] A series of fast camera images is shown in Fig. 1, showing the characteristic azimuthal rotation of the spoke. The spoke was found to rotate in the $\mathbf{E} \times \mathbf{B}$ direction with a speed of 1.2–2.8 km/s, which is substantially less than the local E/B speed of 30 km/s. In-channel Langmuir probes indicated the strongest correlation between density fluctuations and light emissions was near the anode. By increasing the cathode keeper current, which controls the electron supply to the thruster discharge,[23] a transition to high-frequency oscillations replaced the spoke behavior. The cross-field electron transport, characterized by the ratio of the discharge current to the expelled ion current, was observed to decrease when the spoke oscillation was suppressed, suggesting the spoke was altering the cross-field transport. It is then hypothesized that the oscillation mechanism responsible for the rotating light spoke also enhances the local current to the anode.

The similarities of these[15–19,21] findings (with the possible exception of Ref. 21), including an azimuthal perturbation rotating in the $\mathbf{E} \times \mathbf{B}$ direction with a frequency of 10–35 kHz and a velocity slower than the E/B speed, lead us

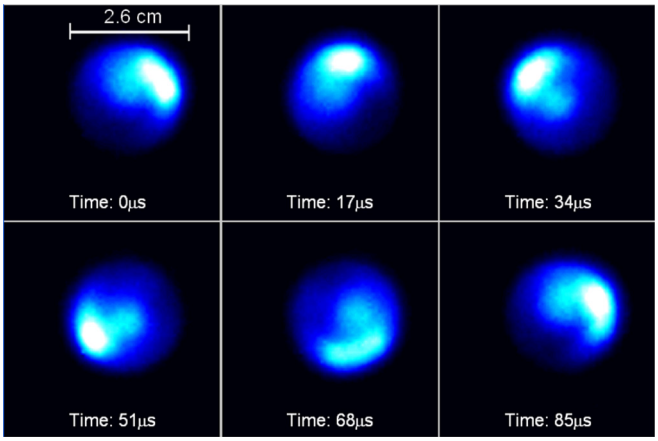

FIG. 1. (Color online) A series of frames displaying the visible light emission from the rotating spoke instability in the 2.6 cm cylindrical Hall thruster. The 15–35 kHz spoke can be seen to rotate in the counter-clockwise direction, which corresponds to the $\mathbf{E} \times \mathbf{B}$ direction. Operating parameters include 250 V discharge bias, 4 sccm Xe mass flow, −2.0 A in the front magnet coils and +2.5 A in the rear coils. Color is artificial.

to suggest the phenomena are related. In this paper, we demonstrate the mechanism of the rotating spoke does alter the cross-field electron transport. Preliminary findings using a segmented anode were presented in Ref. 24. The cross-field current induced by the spoke is directly measured for the first time by installing a segmented anode. Typically, oscillations in the discharge current are monitored, but a continuous anode can only observe longitudinal oscillations, such as the ionization breathing mode. A rotating spoke, which conducts current, would only enhance the current locally (in the azimuthal direction), and thus maintain a constant discharge current. By separating the anode into four azimuthal segments, the current may be observed as a function of position. Measuring the current to each segment in time, synchronized with the fast camera, allows direct identification of the spoke-induced cross-field current. Indeed, we find over half of the total current traverses the rotating spoke, which is large considering the spoke occupies ∼25% of the channel area. To supplement the identification of enhanced cross-field current, the transport mechanism is investigated using emissive and Langmuir probes to determine the phase of the fluctuating potential, temperature, and density relative to the phase of the spoke. The spoke is determined to possess an azimuthal electric field, and a quantitative estimate of the axial electron drift current is approximately equal to the measured spoke current.

II. METHODS

The experiments were performed at the Large Hall Thruster facility at the Princeton Plasma Physics Laboratory, as described elsewhere.[25] The vacuum vessel is equipped with cryogenic pumps, and the background pressure does not exceed 3 μTorr during operation. The basic schematic for the 2.6 cm diameter CHT is shown in Fig. 2.[25] Typical operating parameters include a 4 cm^3/min at standard temperature and pressure (SCCM) xenon mass flow to the anode, 2 SCCM xenon flow to the cathode, 250 V discharge voltage, 2.5 A for the back coils, and −2.0 A for the front coils. The opposite polarity of the fields forms a magnetic cusp near the channel exit and enhances the radial field, as shown in Fig. 3. The field strength near the anode is 850 G. The hollow cathode was operated with a keeper current, I_k, of 1.5–1.8 A. Keeper current is a significant parameter, given the wide variety of oscillatory behavior observed for different settings.[19,23] By enhancing the electron emission from the cathode, the ionization-based breathing mode may be suppressed. Given the close frequency of the breathing mode (typically 10–15 kHz) and the rotating spoke, suppression of the breathing mode simplifies analysis by ensuring the dominant oscillation in the low frequency range is the rotating spoke. At larger keeper current (3.0 A), the spoke oscillation is also suppressed and high frequency (MHz) oscillations appear. A 1.5 A keeper current has been found to be a satisfactory mid-range value for clear spoke observation.[19]

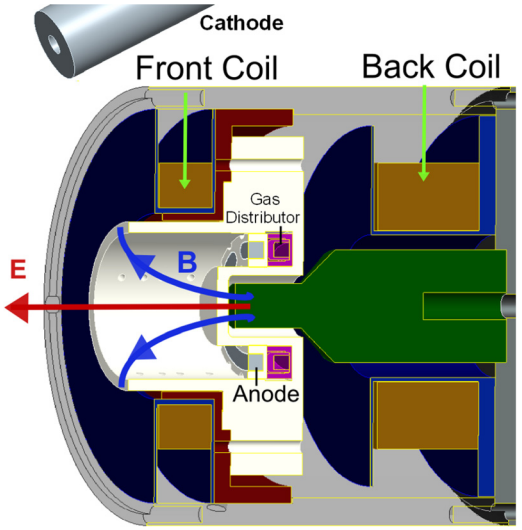

FIG. 2. (Color online) Cross-section view of a cylindrical Hall thruster. Electrons are magnetized and are confined by a combination of the mirror force and the electric field. Ions are not magnetized and are accelerated by the electric field. Segmented anode shown.

A Vision Research Phantom v7.3 fast camera has been used extensively while studying the rotating spoke. The camera is capable of up to 500 000 frames per second (fps), though typical spoke measurements were performed near 200 kfps to achieve a resolution of 64 × 64 pixels. Observations are made 7 m from the thruster and along the axis.

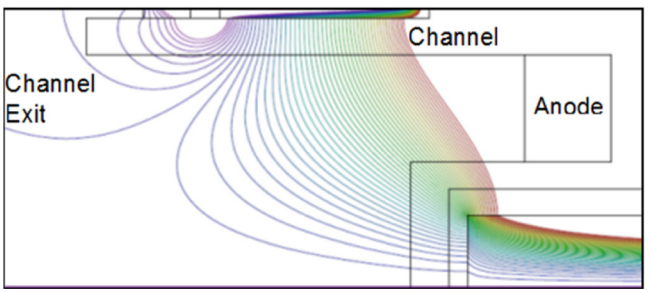

FIG. 3. (Color online) Simulation of the magnetic field in the cusp configuration, with +2.5 A in the back coils and −2.0 A in the front coils. The enhanced cusp shape forms a stronger mirror field. Image is shown about the axis of symmetry. The maximum magnetic field is 875 Gauss and occurs 6 mm from the anode.

Whereas previous configurations[19,25] have used a combined anode and gas distributor, the apparatus for this experiment uses distinct anode and gas distribution components. Two gas inlet tubes extend from the rear of the thruster to the gas distributor positioned behind the anode. Many small holes extend radially from within the gas distributor to provide uniform xenon distribution around the anode. The segmented anode is shown in Fig. 4. A boron nitride base electrically isolates the four anode segments from the gas distributor. The holes around the outer and inner diameter allow the gas to reach the channel from the distributor. The anode segments are 21.6 mm from the channel exit. A single power supply applies the discharge voltage (typically 250 V) between the segmented anode and the hollow cathode, positioned several centimeters beyond the thruster exit. One-ohm resistors in series with each segment allow measurement of the current.

A primary concern was verifying the segmented anode did not alter the operation of the CHT. Impeded gas flow, uncertainties in the axial location of the anode, and modified surface behavior could alter thruster performance. Proper thruster operation was confirmed by comparing characteristic parameters and transitions in oscillation regimes. Indeed, the total discharge current was observed to be 0.85 A, which is typical for this thruster with the cusp field configuration. Similarly, the transitions in breathing mode, spoke, and high frequency oscillations were obtained by modifying the cathode keeper current, and the behavior matched that of previous studies.[19] To confirm no current was being collected by the gas distributor, an attempt was made to start the thruster while biasing the gas distributor instead of the segmented anode. The thruster would not ignite. These verifications suggest that the thruster behavior and ultimately rotating spoke behavior are unaltered by the segmented anode.

One detriment to the segmented anode operation was a dielectric coating, which appeared on the anode over time. The presence of an anode coating is not new[26,27] but can be important when considering the time response of the segments. After several hours of operation, the coating could be observed as discoloration on the stainless steel, and care was taken to remove the coating between experimental efforts. The visual characteristics were similar to those described in Ref. 27, including blue-green and brown hues. Past studies concluded the composition of the dielectric to be oxides of the apparatus, such as stainless steel.[27] The addition of a capacitive component could add a phase delay to the signal, but the 4–7 μs between camera frames is longer than any observed delays. However, care was taken to clean the dielectric coating between experiments to ensure the four segments behaved equally.

For the electrostatic probe measurements, 12 radial holes extend at 4 azimuthal positions and 3 axial positions for probe insertion as can be seen in Fig. 5. The probes are centered above each segment to directly relate the probe signals to the local current. For this set of experiments, emissive probes were placed at the 2 o'clock and 11 o'clock positions while Langmuir probes were placed at the 5 and 8 o'clock positions (as viewed by the fast camera). The axial location of all probes is 5 mm from the anode since previous work determined the spoke to reside near the anode[19] and the fluctuations at this position will most directly relate to the anode current.

The emissive probes extrude a thoriated tungsten filament 1 mm $\times$ 0.5 mm into the plasma while the planar Langmuir probes are positioned flush with the channel wall with an area of 1 mm^2. For hot floating potential measurements, the emissive probe was heated until additional increase in the current did not increase the floating potential. Visible emission from the probe further confirmed it to be operating in the "strongly emitting" regime. Recent measurements indicate the emissive probe floats nearly 2 electron temperatures below the plasma potential,[28] as may be expected in the presence of a space-charge saturated sheath.[29] The Langmuir probes were biased 48 V above ground to operate in the ion saturation current regime, which is a negative bias compared to the 175 V–200 V

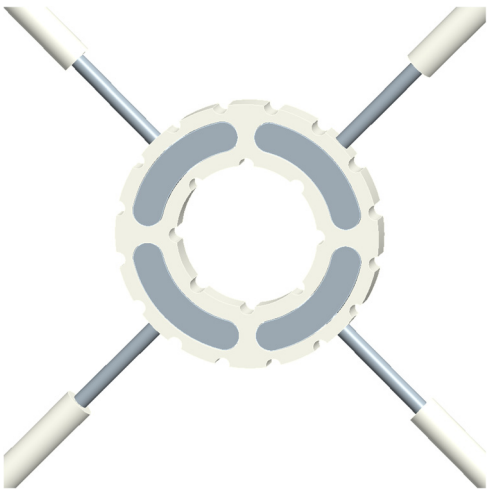

FIG. 4. (Color online) CAD model of the segmented anode assembly. Boron nitride houses the four stainless steel segments. Threaded rods extrude radially to affix the segments and connect the current path. The 8 internal and 16 external semi-circle holes allow gas distribution.

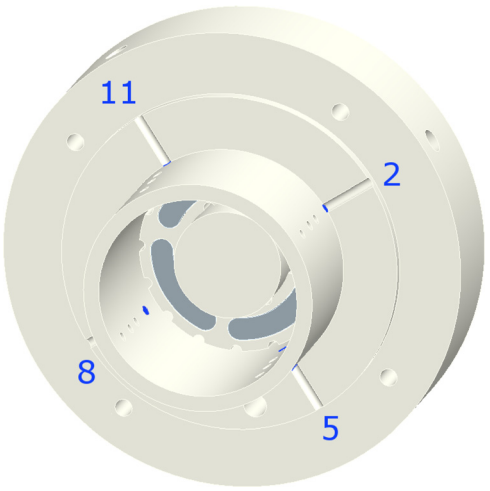

FIG. 5. (Color online) Probe holes in the ceramic channel are visible in this figure. Only those nearest the anode were used in this experiment and may be seen by the circular grooves in the face of the channel and blue highlights. Numbers refer to approximate positions on a clock. Emissive probes were placed at positions 2 and 11 while Langmuir probes were placed at 5 and 8.

space potential. All signals were digitized using LeCroy Waverunner 350 MHz and 500 MHz oscilloscopes. A function generator was used to trigger the fast camera and oscilloscopes, so an individual data set included synchronized measurements of electrostatic probe potentials/currents, segmented anode currents, and fast camera images.

The emissive and Langmuir probes were used to acquire three time-varying parameters in relation to the spoke current: hot floating potential (V_h), cold floating potential (V_c), and ion saturation current (I_{sat}). From these three measurements, we were able to calculate electron temperature (T_e), plasma potential (V_p), electron density (n_e), and azimuthal electric field strength (E_θ) as fluctuating quantities relative to the phase of the spoke-induced current. Ultimately, these quantities yielded an estimate for enhanced transport (drift current I_d) resulting from the fluctuating density and electric field.

To obtain the fundamental measurements V_h, V_c, and I_{sat} relative to the spoke fluctuation, the location of the rotating spoke was digitally identified by a peak in the local segment current. Of course, the current was only used as an identifying mechanism after the current enhancement and strong correlation with light emission was observed as will be described in Sec. III. After identifying potential instances of the spoke traversing an anode segment and electrostatic probe, instances were filtered by rejecting those which occurred too close together or simultaneously on multiple segments. Rejecting peaks in the current which occurred substantially less than the mean spoke period was intended to eliminate periods of non-stationary spoke behavior. Requiring the peak to only occur over one segment excluded stray breathing mode behavior or other non-spoke oscillations. The remaining peaks in anode segment current typically resulted in several hundred spoke periods per dataset. The characteristic spoke current, V_h, V_c, and I_{sat} were obtained by averaging over a time window about the current peak chosen based on the mean spoke period.

To extract electron temperature from the hot and cold floating potentials, it was assumed[28,30]

$$\begin{aligned} V_h &= V_p - 2T_e, \\ V_c &\approx V_p - 5.77T_e. \end{aligned} \tag{1}$$

Subtraction of the two traces then yielded 3.8 T_e. This method is different from obtaining temperature by sweeping the voltage on an electrostatic probe to obtain an I-V characteristic, but determination of the temperature as a function of time would require high-frequency sweeps, so this method provides the best available estimate. The results obtained are smaller than swept-temperature measurements in previous studies[31] by approximately a factor of 3. One reason may be the probe position, as Ref. 31 used biased planar probes flush with the channel wall while the above method uses the emissive probe extruded in the plasma. Another possible difference is the non-Maxwellian electron distribution present in the thruster. Even in the presence of non-Maxwellian distributions, because the temperature measurements will be used to calculate density from the ion saturation current, we are more interested in the lower temperature population which affects the Bohm velocity than the higher temperature population which can influence temperature measurements using a swept bias.

To retrieve the best estimate of the plasma potential, 2 T_e as determined above was added to the hot floating potential. From the plasma potential estimate, the azimuthal component of the electric field was extracted by assuming the spoke velocity and parameters to be constant (on average) as the spoke moves across the emissive probe. An azimuthal electric field may then be calculated by using the spoke velocity to get from a time derivative to a space derivative

$$E_\theta = -\frac{dV_p}{d\theta} = -\frac{dV_p}{dt}\left(\frac{d\theta}{dt}\right)^{-1} = -\frac{1}{v_{spoke}}\frac{dV_p}{dt}, \tag{2}$$

where v_{spoke} is the average velocity of the spoke, taken here to be 930 m/s, which corresponds to an 11 kHz spoke.

Plasma density as a function of time was calculated from the ion saturation current to the biased Langmuir probe, using the expression for the Bohm ion flux at the sheath edge as follows:

$$I_{sat} = 0.6 q_e n_e A_p c_s, \tag{3}$$

where q_e is the electron charge, n_e is the electron density in the bulk plasma, A_p is the probe area, and c_s is the ion sound speed determined using T_e and the xenon mass. Equation (3) assumes a small, planar sheath compared to the probe dimensions and takes the ions to be drifting to the biased probe with the Bohm velocity while repelling all electrons. The presence of a non-Maxwellian electron energy distribution may allow the ion saturation to deviate from this simple estimate. In measuring the ion saturation current, it was discovered that a small, negative DC offset was present in the data. The offset was determined to be approximately 10% of the maximum saturation current. Statistical uncertainties were on the order of 20%, so the offset is notable but not the dominant source of error.

Probe measurements inside the channel must be performed carefully to prevent perturbing the plasma environment.[32] Biasing the Langmuir probe at the wall alters the floating sheath geometry and collects particles, which would otherwise be in the plasma. The extruding emissive probe extends into the bulk of the plasma and (despite floating) can alter the electron distribution function through emissions. Emissive probes are also delicate and may quickly be destroyed in the harsh plasma. Probe measurements were possible because of the near-anode axial location, as has been achieved in previous studies.[29,33] This region is before the acceleration zone, and thus the plasma is less likely to harm the probes and thruster operation will be less sensitive to small space potential perturbations. The discharge current remained near 0.85 amps, even with the emitting probes and while collecting ion saturation current. To test for azimuthal perturbations, we measured the floating potential of a probe directly adjacent to the emitting probe in the $\mathbf{E} \times \mathbf{B}$ direction. The floating potential showed no change with the probe emitting or cold, confirming no significant perturbation to the steady state potential.

The final calculated quantity relative to the spoke current is a simple estimate of the enhanced transport due to the electric field and density fluctuations. The perturbed electric field E_θ was found to be in the direction such that the $\mathbf{E}_\theta \times \mathbf{B}$ drift is towards the anode, as will be shown in Sec. III. The net contribution to the current, I_{drift}, as the spoke traversed the anode segments and electrostatic probes was estimated as

$$I_{drift} = ev_d n_e A_s, \tag{4}$$

where v_d is the $\mathbf{E} \times \mathbf{B}$ drift velocity of the electrons and A_s is the area of the anode segment. This quantity is a useful measure of whether the fluctuating quantities explain the enhanced cross-field transport through the rotating spoke or whether some other mechanism is responsible.

III. RESULTS

The fast camera, segmented anode, and electrostatic probes allowed direct measurements of the cross-field current conducted through the rotating spoke for the first time. The spoke was found to enhance the current as camera and segmented anode measurements indicate over half of the total current traverses the spoke. The breathing mode was successfully suppressed using enhanced cathode keeper current, isolating the rotating spoke as the dominant oscillation. Electrostatic probe measurements near the anode provided more detailed measurements of the phenomena, providing characteristic density, potential and temperature fluctuations relative to the enhanced current. The phase of the density and potential relative to the spoke current indicate a perturbed electron drift towards the anode. As a simple qualitative model of the transport mechanism, a drift current was estimated using the perturbed $\mathbf{E} \times \mathbf{B}$ velocity and the density profile. The resulting drift current is approximately equal to the spoke current when the spoke is centered on an anode segments.

Using the segmented anode, the current through the spoke has been measured to be over 50% of the anode current, as shown in Fig. 6. Specifically, we find 56% of the total current to be conducted through the spoke with a standard deviation of 13%. Due to variation in the spoke behavior and the possibility of a low amplitude breathing mode, the waveform of the spoke current was determined by averaging over several hundred cycles and averaged across the four segments of the anode. The spoke was identified digitally by finding peaks in the smoothed current, requiring a minimum peak spacing of half the average spoke frequency, and checking that the anode segment with the peaking current was also collecting the most current of the four segments. The time axis has been normalized to the spoke period, which ranges from 30 μs to 80 μs. During an individual 10 ms data set, the spoke frequency and period is relatively constant (varies 25% of the mean), but operation over several hours can include spoke behavior over the entire frequency range, likely due to changes in thruster temperature and impurity levels. Thus, comparisons across datasets are most insightful if normalized to the spoke period.

The current to the individual segments was found to be highly correlated with the local intensity as observed by the fast camera. The time series of the average brightness over the quarter of the thruster centered on a given segment was compared to the time series of the segment current. The cross correlation was typically 0.9, indicating the strong similarity of the signals, so relying purely upon the segmented anode current proved effective at identifying the spoke location, and the fast camera was not used in electrostatic probe measurements.

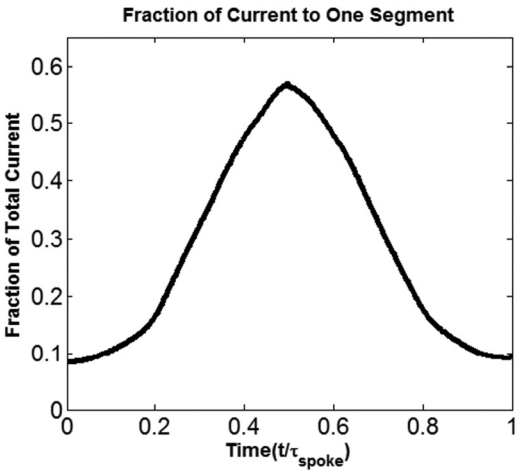

FIG. 6. Characteristic waveform of the current through the rotating spoke to a single segment of the anode. The current rises and falls as the spoke becomes centered over the segment, then passes onto the next. The trace was determined by averaging over several hundred spoke cycles. The time axis is normalized to the spoke period, which ranges from 30 μs to 80 μs. The maximum is 0.57 with a standard deviation of 0.13.

The measurement of enhanced cross-field transport represents the first direct measurement of the rotating spoke fluctuation-induced current. Over half of the total current is localized to one quarter of the channel area. While the measurements of enhanced current are interesting in themselves, probe measurements were used to investigate the transport mechanism. Fig. 7(a) shows the measured potential, density, and temperature fluctuations relative to the characteristic spoke current. All quantities are normalized for phase comparison. The density obtains a maximum of 3.1×10^{12} cm^{-3} $\pm 6 \times 10^{12}$ cm^{-3}, within a microsecond of the peak in the spoke-induced current. The temperature fluctuates between a maximum of 7.1 ± 0.5 eV and minimum of 2 eV, and the plasma potential between 230 ± 2 V and 197 V.

Across the measurements, the phase of the fluctuations relative to the spoke-induced current was more consistent than the magnitude of the oscillations. Fig. 7(a) shows the density is closely in-phase with the spoke current, whereas the potential and temperature fluctuations are approximately 135° shifted. For transport considerations, it is important to note that the potential is not completely out of phase (180°), since this would result in no net current induced by the fluctuation. In magnitude, we observe the density fluctuates on order unity while temperature is ~50% of the mean and plasma potential varies 33 V or 15% of the mean.

The phase of the potential fluctuation indicates an azimuthal electric field, which causes a net electron drift in the direction of the anode segment. The drift velocity may then be calculated according to Eq. (4) using the measured

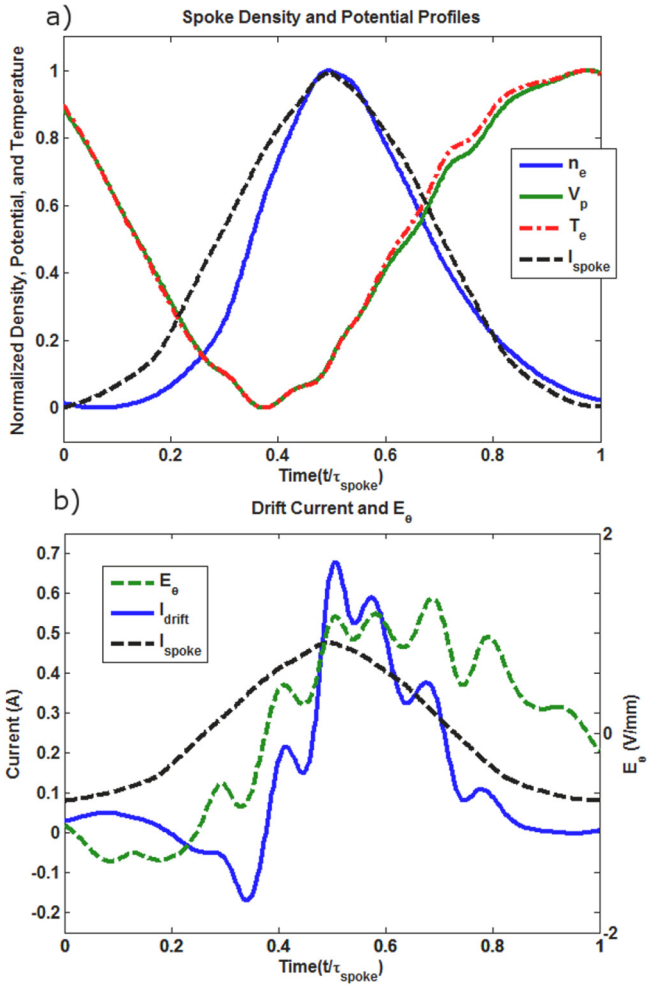

FIG. 7. (Color online) (a) Normalized electron density, temperature, and potential fluctuations relative to the rotating spoke-induced current. The density has a maximum of $3.1 \pm 0.6 \times 10^{12}$ cm^{-3}, the temperature a maximum of 7.1 ± 0.5 eV, and the potential a maximum of 230 ± 2 V. (b) Azimuthal electric field deduced from the plasma potential and fluctuation-induced drift current relative to the segmented anode-measured current.

azimuthal field and the radial component of the magnetic field, taken to be constant at 760 G, as determined using field simulation software. Indeed, we find a significant drift velocity directed towards the anode when the spoke is present. The drift velocity peaks at 15 km/s, which is fast enough to traverse the 5 mm gap between the measurement location and the anode during the spoke presence. The electric field and current caused by the resulting drift are shown in Fig. 7(b).

The drift current peaks at 0.67 A within 1 μs of the peak in spoke current, which has a magnitude of 0.48 A. The drift current exceeds the magnitude of the spoke current, but between 20% statistical uncertainty in the drift current (dominated by the uncertainty in the density measurement) and 25% uncertainty in the spoke current, the error bars overlap. Despite using a simple drift-current model for the fluctuation-induced current, the results are in reasonable agreement. The similarity of the results indicates the macroscopic fluctuations as measured by the electrostatic probes are responsible for the dominant contribution to the spoke-induced current. This is in contrast to, for instance, small-scale turbulence occurring within the spoke which enhanced transport. While small-scale turbulence may influence the development of the spoke instability and may be responsible for the discrepancies between the drift current and the spoke-induced current, it appears that the macroscopic fluctuations in density and potential are largely responsible for the induced current. The drift-current estimate serves to supplement the segmented anode measurement by calculating fluctuation-induced transport in a less direct manner, and the agreement improves trust in both the probe and anode measurements.

While the peaks of the currents agree to a reasonable degree, two discrepancies are apparent in Fig. 7(b). For one, the spoke-induced current rises and falls symmetrically about the half-period, whereas the drift current is more prevalent in the later times. Additionally, a higher-frequency oscillation is present on the electric field and drift current, which does not appear on the smooth, spoke current waveform. The asymmetry in the drift current arises from the potential fluctuation, which drifts electrons away from the anode for the initial portion of the fluctuation and towards the anode in the middle and late phase. The symmetry of the spoke-induced current is not captured in the simple drift-current model and is perhaps due to small-scale turbulent fluctuations for the initial current contribution. The high-frequency behavior may not be present upon averaging over a larger number of samples, but it is unclear at this time whether it is physical and not included in the model or an artifact of the data sets.

Despite the preceding considerations, the electrostatic probe measurements serve to validate the segmented anode measurements and provide estimates of fundamental fluctuating quantities, such as density, temperature, and potential, against which a more robust theory of the rotating spoke oscillation may be compared.

IV. CONCLUSION

In summary, the cross-field electron transport induced by the rotating spoke was directly measured for the first time using a segmented anode. On average, over 50% of the total current is conducted by the spoke, which is large given the spoke area of one quarter the channel area. The transport mechanism was estimated using electrostatic probes and a drift-induced current model. At the maximum spoke current and drift current (when the spoke is centered on the anode segment), the measurements are in reasonable agreement.

Remaining questions regard the source of the spoke instability. It is not obvious that a $m = 1$ mode should dominate the spoke, and indeed other experiments have revealed higher-mode structure.[18] Moreover, the relatively low speed of the spoke rotation requires explanation. Comparison with the local field values of $E = 20$ V/cm[32] and $B = 850$ G indicate the spoke velocity of 2 km/s is 1/10 of the local $E \times B$ velocity of 20 km/s, thus the mechanism for establishing the density and potential perturbation are of theoretical interest. While knowledge of the true $E \times B$ speed is complicated by uncertainty in the local electric field and non-equipotential magnetic field lines, these effects may alter the estimate by a

factor of 2 while a difference of a factor of 10 exists. Moreover, the dip in the spoke potential would suggest the local $E \times B$ speed is even larger at the spoke location (estimating the axial electric field as the anode potential minus the spoke potential divided by the separation distance). The common feature of sub-$E \times B$ velocity among the azimuthal perturbation studies[15–19] makes it an important emphasis for study. The low velocity has been suggested to be related to the critical ionization velocity,[15,17] but the match is inexact and mechanism unconfirmed. It is then of interest to understand the mechanism which determines the velocity and establishes a density perturbation, which does not rotate at the E/B speed.

The presence of the fluctuating temperature also suggests the mechanism may be ionization related, such as an azimuthal manifestation of the breathing mode. Axial breathing modes have been studied,[34] but it is unclear whether a similar phenomena is possible, which propagates an ionization front in the azimuthal direction while conducting electrons axially. In support of this notion, recent 3-D PIC simulations have found azimuthally propagating waves, which deplete neutrals and resemble the rotating spoke oscillation.[35] Further study will be required to confirm matching fluctuation parameters and theoretical understanding of the rotating spoke mechanism. Experimental and theoretical studies on an annular thruster have found azimuthal propagations with in-phase temperature and potential fluctuations which result in ionization and locally enhanced current.[36]

Ultimately, the enhanced transport through the spoke degrades CHT efficiency and understanding the instability mechanism could allow suppression of the spoke mode without the use of the keeper current. For instance, unequal biasing of the segmented anode with opposite phasing of the spoke rotation may suppress the enhanced spoke transport without the onset of worse fluctuations, leading to decreased current and improved CHT efficiency. More fundamentally, the appearance of the perturbation in many thrusters means understanding the rotating spoke is important for basic cross-field transport and perhaps beyond Hall thrusters to more general $E \times B$ devices. Even in the fusion setting, thorough understanding of fluctuation-induced transport and plasma instabilities is critical to optimizing plasma confinement.

ACKNOWLEDGMENTS

The authors would like to thank J. Parker, M. Griswold, J. C. Gayoso, J. P. Sheehan, K. Matyash and R. Schneider for their assistance and helpful discussions. This work was performed under the support of a DOE—Fusion Energy Sciences Fellowship. This manuscript has been authored by Princeton University and collaborators under Contract Number DE-AC02-09CH11466 with the U. S. Department of Energy with additional support from the Air Force Office of Scientific Research (AFOSR).

[1]M. Keidar and I. I. Beilis, IEEE Trans. Plasma Sci. **34**, 804 (2006).
[2]J. E. Maggs, T. A. Carter, and R. J. Taylor, Phys. Plasmas **14**, 052507 (2007).
[3]Q. Quraishi, S. Robertson, and B. Walch, Phys. Plasmas **9**, 3264 (2002).
[4]V. V. Zhurin, H. R. Kaufman, and R. S. Robinson, Plasma Sources Sci. Technol. **8**, R1 (1999).
[5]A. I. Morozov and A. P. Shubin, Pisma v Zhurnal Tekhnicheskoi Fiziki **10**(1), 28 (1984).
[6]J. C. Adam, J. P. Boeuf, N. Dubuit, M. Dudeck, L. Garrigues, D. Gresillon, A. Heron, G. J. M. Hagelaar, V. Kulaev, N. Lemoine, S. Mazouffre, J. Perez Luna, V. Pisarev, and S. Tsikata, Plasma Phys. Controlled Fusion **50**, 124041 (2008).
[7]J. P. Boeuf and L. Garrigues, J. Appl. Phys. **84**, 3541 (1998).
[8]N. B. Meezan, W. A. Hargus, Jr., and M. A. Cappelli, Phys. Rev. E **63**, 026410 (2001).
[9]E. Y. Choueiri, Phys. Plasmas **8**, 1411 (2001).
[10]M. J. Burin, G. R. Tynan, G. Y. Antar, N. A. Crocker, and C. Holland, Phys. Plasmas **12**, 052320 (2005).
[11]D. Milligan, D. Gestal, and O. Camino, J. Br. Interplanet. Soc. **61**, 466 (2008).
[12]Y. Raitses and N. J. Fisch, Phys. Plasmas **8**, 2579 (2001).
[13]A. Smirnov, Y. Raitses, and N. J. Fisch, Phys. Plasmas **14**, 057106 (2007).
[14]N. J. Fisch, Y. Raitses, and A. Fruchtman, Plasma Phys. Control. Fusion **53**, 124038 (2011).
[15]G. S. Janes and R. S. Lowder, Phys. Fluids **9**, 1115 (1966).
[16]Y. V. Esipchuk, A. I. Morozov, G. N. Tilinin, and A. V. Trofimov, Sov. Phys. Tech. Phys. **43**, 1466 (1973).
[17]E. Chesta, C. M. Lam, N. B. Meezan, D. P. Schmidt, and M. A. Cappelli, IEEE Trans. Plasma Sci. **29**, 582 (2001).
[18]M. McDonald, C. Bellan, B. A. St. Pierre, and A. D. Gallimore, 47th AIAA/ASME/SAE/ASEE Joint Propulsion Conference and Exhibit, San Diego, CA, July 31–August 3, 2011, Paper No. AIAA-2011-5810.
[19]J. B. Parker, Y. Raitses, and N. J. Fisch, Appl. Phys. Lett. **97**, 091501 (2010).
[20]E. Mobius and R. W. Boswell, Geophys. Res. Lett. **6**, 29, doi:10.1029/GL006i001p00029 (1979).
[21]A. W. Smith and M. A. Cappelli, Phys. Plasmas **16**, 073504 (2009).
[22]C. L. Ellison, Y. Raitses, and N. J. Fisch, IEEE Trans. Plasma Sci. **39**(11), 2950 (2011).
[23]Y. Raitses, A. Smirnov, and N. J. Fisch, Phys. Plasmas **16**, 057106 (2009).
[24]C. L. Ellison, Y. Raitses, and N. J. Fisch, 52nd Annual Meeting of the APS Division of Plasma Physics, Abstract Log Number DPP10-2010-001225, Session PP9, November 8–12, 2010.
[25]A. Smirnov, Y. Raitses, and N. J. Fisch, J. Appl. Phys. **92**, 5673 (2002).
[26]L. Dorf, Y. Raitses, and N. J. Fisch, Appl. Phys. Lett. **84**, 1070 (2004).
[27]L. Dorf, Y. Raitses, and N. J. Fisch, J. Appl. Phys. **97**, 103309 (2005).
[28]J. P. Sheehan, Y. Raitses, N. Hershkowitz, I. Kaganovich, and N. J. Fisch, Phys. Plasmas **18**, 073501 (2011).
[29]L. Dorf, Y. Raitses, and N. J. Fisch, Rev. Sci. Instrum. **75**, 1255 (2004).
[30]I. H. Hutchinson, *Principles of Plasma Diagnostics* (Cambridge University Press, Cambridge, England, 2002).
[31]A. Smirnov, "Experimental and theoretical studies of cylindrical Hall thrusters," Ph.D. dissertation (Princeton University, Princeton, NJ, 2006).
[32]T. Ito and M. A. Cappelli, Appl. Phys. Lett. **94**, 211501 (2009).
[33]A. Smirnov, Y. Raitses, and N. J. Fisch, Phys. Plasmas **14**, 057106 (2007).
[34]S. Barral and E. Ahedo, Phys. Rev. E **79**, 046401 (2009).
[35]K. Matyash, R. Schneider, O. Kalentev, Y. Raitses, and N. J. Fisch, in *Proceedings of the IEPC-2011-070*, 2011.
[36]A. N. Vasselovzorov, E. D. Dlougach, A. A. Pogorelov, E. B. Svirskiy, and V. A. Smirnov, in *Proceedings of the IEPC-2011-060*, 2011.